




Simultaneous measurement of in-plane and interfacial thermal conductivity of isotopically labeled bilayer graphene

Yang Zhang ^{1,2,3,*} Qiancheng Ren,^{1,2,3,*} Jiayuan Fang,^{1,2,3} Jinglan Liu,⁴ Suhao Wang ^{1,3},
Jizhou Song,^{1,3} and Pei Zhao ^{1,2,3,†}

¹State Key Laboratory of Fluid Power and Mechatronic Systems, Zhejiang University, Hangzhou 310027, People's Republic of China

²Center for X-Mechanics, Zhejiang University, Hangzhou 310027, People's Republic of China

³Department of Engineering Mechanics, Zhejiang University, Hangzhou 310027, People's Republic of China

⁴School of Science, Qingdao University of Technology, Qingdao 266520, People's Republic of China



(Received 26 July 2023; revised 19 December 2023; accepted 2 January 2024; published 22 January 2024)

The thermal properties of bilayer graphene (BLG) play a crucial role in the advancement of its promising electronic devices. However, the measurement of thermal conductivity using current techniques faces obstacles due to the low temperature gradient both in plane and across the interface in the sample. Here we present an approach to simultaneously explore the in-plane and interfacial thermal conductivity of chemical vapor deposited AB-stacked BLG by utilizing an isotope labeling assisted Raman spectroscopic technique. By applying the modified heat diffusion model, we acquire the interfacial thermal conductivity of isotopically labeled AB-stacked BLG of $105 \pm 3 \text{ MW}/(\text{m}^2 \text{ K})$, whereas we find the in-plane thermal conductivity of each layer is reduced compared with their monolayers. This technique demonstrates strong support for advancing the BLG thermal engineering research as well as a potential of extending to other two-dimensional systems.

DOI: [10.1103/PhysRevB.109.L041407](https://doi.org/10.1103/PhysRevB.109.L041407)

The thermal properties of bilayer graphene (BLG) have become an increasingly critical issue, because the stack has demonstrated unconventional behaviors and plays a significant role in electronic devices [1–4]. Although extensive theoretical and simulation studies have been conducted [5–8], to date there has been little experimental evidence to explore its thermal conductivity. Actually, there are various methods for measuring thermal conductivity of two-dimensional (2D) materials: for example, Pettes *et al.* utilized a traditional approach of two micro-resistance thermometers to measure BLG and reported that its in-plane thermal conductivity (K) is influenced by the presence of polymeric residues [9]; the time-domain thermoreflectance (TDTR) method is a more commonly used method for measuring the interfacial thermal conductivity (G) for 2D stacks [10–12], although the presence of the deposited metal layer may impede the out of plane (ZA) phonons [13,14].

Over the past 10 years, Raman spectroscopy has been widely used to study the in-plane thermal conductivity of graphene since the first report of K of over $5000 \text{ W}/(\text{m K})$ by Balandin *et al.* [15], followed by a series of works from Ruoff's group (Cai *et al.* [16] and Chen *et al.* [17,18]). However, there are currently few works to simultaneously report K and G for BLG [19,20]. The crucial challenge is that the Raman spectra signals of these layers which consist of identical atoms overlap. Therefore, to fully explore the potential of Raman spectroscopy, it is essential to develop a more effective system from the view of material design to differentiate the

Raman signals from the two layers as well as a corresponding heat diffusion model to depict them.

In this work, we present an approach to simultaneously measure the in-plane and interfacial thermal conductivity of isotopically labeled AB-stacked BLG by utilizing an isotope labeling assisted Raman spectroscopic technique. BLG with a top layer composed of ^{12}C atoms and a bottom layer of ^{13}C atoms is synthesized by chemical vapor deposition (CVD), and their distinctive Raman feedback on featured peaks allows the temperature of each layer heated by the laser be determined. Based on a modified heat diffusion model, the G is numerally calculated as $105 \pm 3 \text{ MW}/(\text{m}^2 \text{ K})$ and K of each layer is found significantly reduced compared with their monolayers. We hope these findings can provide support for the study of phonons and promote the development of thermal management for 2D materials.

Preparation details. BLG was synthesized on commercially available $25 \mu\text{m}$ thick Cu foils [#46986, Alfa Aesar (China) Chemical Co., Ltd.] by the CVD method [21]. After growing, it was transferred onto an Au-coated SiO_2/Si substrate with a series of holes by the acrylate terpolymer-assisted wet transfer approach [22]. The Au layer was deposited by physical vapor deposition (PVD) (Discovery-635, Denton Co., Ltd). BLG was characterized by an optical microscope (OM) (Olympus BXFM-ILHS, Olympus Co., Ltd.), Micro-Raman spectroscopy (LabRAM HR Evolution, Horiba Co., Ltd.), a scanning electron microscope (SEM) (S-3400 I, Hitachi Co., Ltd.), and a transmission electron microscope (TEM) (JEM-2100, Jeol Co., Ltd.). To measure the laser absorption (α) of respective layers in BLG, monolayer graphene consisting of 99.9% $^{12}\text{CH}_4$ and 99% $^{13}\text{CH}_4$ was respectively transferred onto a transparent glass substrate. A power meter

*These authors contributed equally to this work.

†peizhao@zju.edu.cn

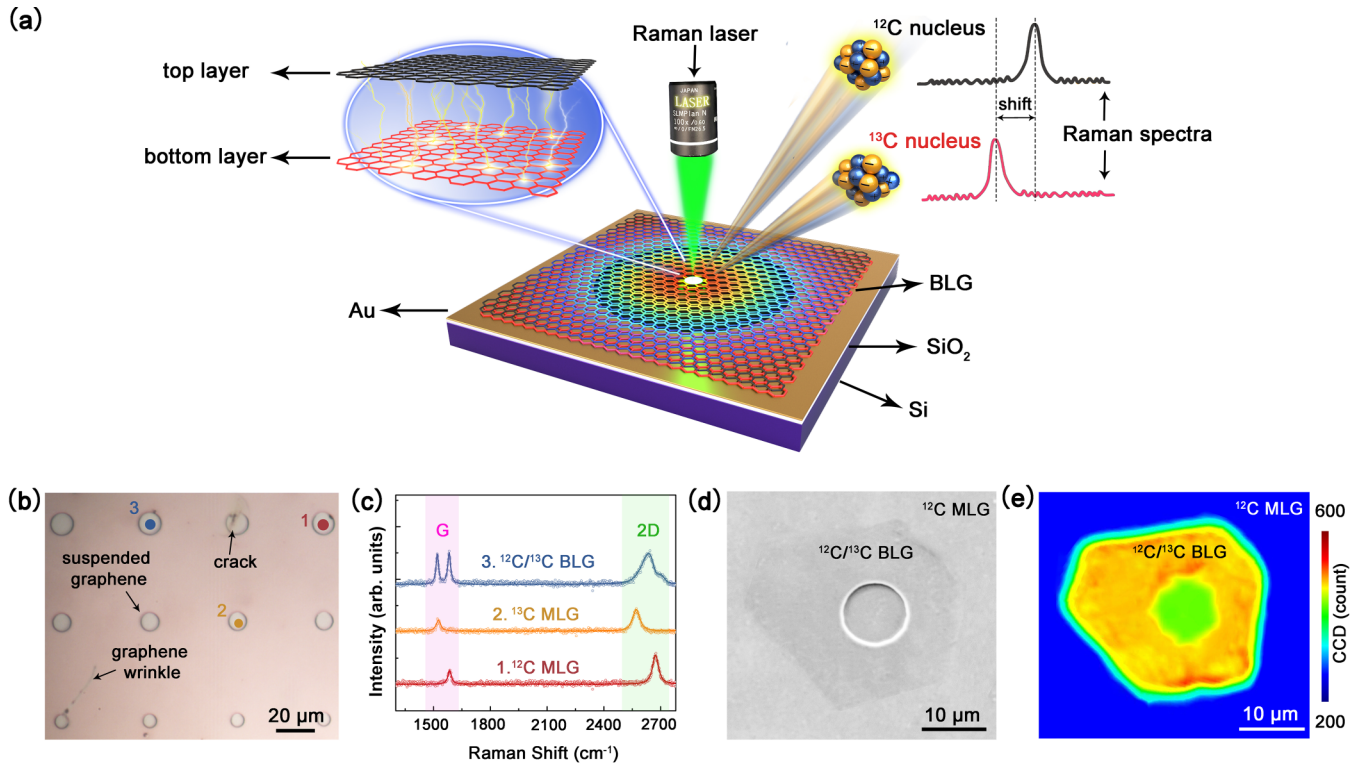


FIG. 1. Schematic diagram of the measurement setup and characterizations of $^{12}\text{C}/^{13}\text{C}$ BLG. (a) Schematic diagram of the measurement setup. (b) OM image of the BLG. (c) Raman spectra obtained from (b). (d) SEM image of region 3 in (b). (e) Intensity contour of the $\sim 1525\text{ cm}^{-1}$ Raman peak scanned from (d).

was respectively placed above and below the graphene/glass to measure $P_{\text{above}1}$ and $P_{\text{below}1}$, and the measurements of $P_{\text{above}2}$ and $P_{\text{below}2}$ were also recorded without graphene covering. α was calculated as $\alpha = \frac{P_{\text{above}1} - P_{\text{below}1} - P_{\text{above}2} - P_{\text{below}2}}{P_{\text{above}1}}$.

Experimental setup. To eliminate phonon inhibitions caused by the substrate, a SiO_2/Si substrate with patterned holes was fabricated (Fig. S1 in the Supplemental Material [23]), and a 150 nm thick Au layer was coated as the heat sink [Fig. 1(a)]. A 532-nm laser focused on the center of the suspended BLG was used as a heating source, and the generated heat caused a redshift of the Raman peaks in the spectrum [24]. For homogeneously layered 2D materials, the Raman spectra from the two layers are overlapped, making the acquirement of temperatures in each layer a challenge. However, for our BLG sample, ^{13}C atoms are introduced to the bottom layer [21], whose greater weight leads to a pronounced redshift of Raman peaks compared to the top layer, which makes it possible to simultaneously analyze the in-plane and interfacial thermal conductivity of BLG [25].

Figure 1(b) presents an OM image of BLG on the Au-coated SiO_2/Si substrate, and Raman spectroscopy was employed as shown in Fig. 1(c). The peak shapes and intensity ratios of regions 1 and 2 indicate these are monolayer graphene (MLG) [26], but graphene in region 3 exhibits significant Raman fingerprints of AB-stacked $^{12}\text{C}/^{13}\text{C}$ BLG [27]. The Raman peaks in bilayer graphene are not a simple summation of the monolayer spectra, particularly in the case of the 2D peak, which arises from the double resonance of $i\text{TO}$ phonon modes in the two layers [27]. Moreover, the introduction of isotopes results in a difference in the phonon energy,

resulting in the 2D peak actually decomposing into eight components as shown in Fig. S2 [23]. The SEM image in Fig. 1(d) further confirms the double layer nature, and Fig. 1(e) also indicates its uniformly high quality both over the hole and around it. In the following study, only AB-stacked $^{12}\text{C}/^{13}\text{C}$ BLGs with morphological and spectral characteristics similar to those in region 3 were measured.

Thermal measurement. To acquire the temperature of each layer under different laser powers as shown in Fig. 2(a), it is necessary to perform a temperature calibration by placing samples on a heat stage (Fig. S3) [23]. The calibration results are shown in Fig. 2(b), and the temperature coefficients (χ_T) for the ^{12}C top layer as $-0.311 \pm 0.02\text{ cm}^{-1}/\text{K}$ and for the ^{13}C bottom layer as $-0.288 \pm 0.03\text{ cm}^{-1}/\text{K}$ were derived using a first-order linear fit [28]. To fulfill the requirement of the heat diffusion model derived later, the calibration using the other two objective lenses was performed, and the measured methodology of the beam waist radii for the lasers through three lenses is shown in the Supplemental Material [23]. Figure S4 and Table S1 show the three measured beam waist radii. After obtaining χ_T in Fig. 2(b) [23], the temperature of each graphene layer (T_m) under different laser powers in Fig. 2(c) can be determined using the following equation,

$$T_m = T_r + \frac{\omega_m - \omega_r}{\chi_T}, \quad (1)$$

where T_r and ω_r are the corresponding temperature and Raman peak position at room temperature, and T_m and ω_m are the corresponding temperature and Raman peak position under the measured power, respectively. Figure 2(d) displays the

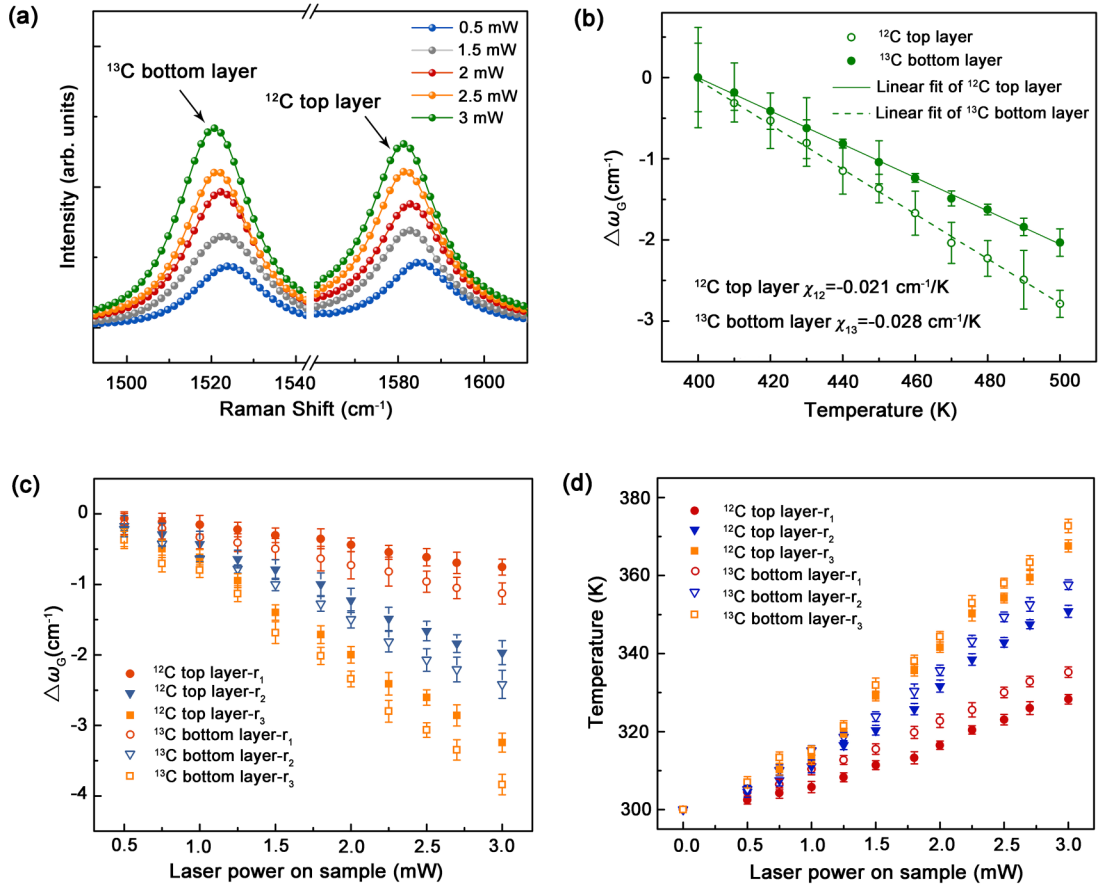


FIG. 2. Raman G peak shifts of AB-stacked $^{12}\text{C}/^{13}\text{C}$ BLG. (a) The ^{12}G and ^{13}G peak positions for BLG excited by different laser powers. (b) The ^{12}G and ^{13}G peak shifts of BLG during the calibration process. (c) The ^{12}G and ^{13}G peak shifts and (d) measured temperatures of BLG under different laser powers and objective lenses.

corresponding local temperatures of each layer in the BLG and the differences obtained by different objective lenses can be attributed to the varying effective heating areas [19]. The analysis of the full widths at half maximum (FWHMs) (Fig. S5 [23]) and the peak positions of the G peaks (Fig. S6) in the Supplemental Material reveal the “additional” strain during the measurements is approximately one order of magnitude smaller than the measured value [23]; any “additional” doping effect has also been taken into account.

Heat diffusion model. After determining the individual temperatures of each layer in BLG, a modified heat diffusion model to obtain G and K was developed. When a laser beam is focused on the center of the suspended BLG, both layers experience a temperature increase due to the laser absorption. The laser absorption values (α) of the ^{12}C top layer and the ^{13}C bottom layer are 3.8% and 2.4%, respectively, which is assumed to be independent of the temperature [29]. Neglecting the heat convection and radiation to the environment, the temperature distribution within the BLG is

$$\begin{aligned} \frac{1}{r} \frac{d}{dr} \left(r \frac{dT_{12}}{dr} \right) - \frac{g}{h\kappa_{12}} (T_{12} - T_{13}) + \frac{q_{12}}{\kappa_{12}} &= 0, \\ \frac{1}{r} \frac{d}{dr} \left(r \frac{dT_{13}}{dr} \right) - \frac{g}{h\kappa_{13}} (T_{13} - T_{12}) + \frac{q_{13}}{\kappa_{13}} &= 0, \end{aligned} \quad (2)$$

where r is the radial distance from the center of the laser beam, T is the temperature of graphene, g is the overall interfacial thermal conductivity, κ is the overall in-plane thermal conductivity, $h = 0.335$ nm is the thickness of MLG, and q is the volumetric heat from the laser. The subscripts of “12” and “13” represent the variables of the ^{12}C top layer and the ^{13}C bottom layer, respectively. The influence of the air disturbance around graphene on the results is neglected, as discussed in detail in the Supplemental Material [23]. The detailed solution of Eq. (3) can be found in the Supplemental Material [23], and the temperature distribution of each layer is written as

$$\begin{aligned} T_{12}(r) &= \int \frac{\int \left(-\frac{g}{hp^2\kappa_{12}} M - \frac{q_{12}}{p^2\kappa_{13}} \right) dz}{z} dz + C_1, \\ T_{13}(r) &= \int \frac{\int \left(-\frac{g}{hp^2\kappa_{12}} M - \frac{q_{13}}{p^2\kappa_{13}} \right) dz}{z} dz + C_2, \end{aligned} \quad (3)$$

where C_1 and C_2 are constants that can be solved by the boundary conditions of $T_{12}|_{r=R} = T_r$ and $T_{13}|_{r=R} = T_r$, where T_r represents the room temperature, in which R is the radius of the hole. For the discussion on the reliability of this boundary condition assumption, please refer to the Supplemental Material [23]. Variables z , p , and r follow the relation of $z = \left[\frac{g(\kappa_{12} + \kappa_{13})}{h\kappa_{12}\kappa_{13}} \right]^{0.5} r = pr$, and M denotes the temperature

difference between the two layers. Therefore, for the measured temperature values each layer can be expressed as

$$T_{12m} = \frac{\int_0^{z_R} T_{12} \exp\left(-\frac{z^2}{z_0^2}\right) z dz}{\int_0^{z_R} \exp\left(-\frac{z^2}{z_0^2}\right) z dz},$$

$$T_{13m} = \frac{\int_0^{z_R} T_{13} \exp\left(-\frac{z^2}{z_0^2}\right) z dz}{\int_0^{z_R} \exp\left(-\frac{z^2}{z_0^2}\right) z dz}, \quad (4)$$

where $z_0 = pr_0$, where r_0 is the radius of the laser beam, and $z_R = pR$.

We define the measured differential thermal resistance as $\Delta R_m \equiv \frac{T_{12m} - T_{13m}}{Q}$, where Q is the total heat from the laser on each graphene layer; $R_m = \frac{\partial T_m}{\partial Q}$ instead of $R_m = \frac{T_m}{Q}$ was used to avoid the measured errors. Then R_m can be experimentally derived using

$$\Delta R_m = \frac{\partial T_{12m}}{\partial \omega_{12}} \frac{\partial \omega_{12}}{\partial Q} - \frac{\partial T_{13m}}{\partial \omega_{13}} \frac{\partial \omega_{13}}{\partial Q}$$

$$= \chi_{12P} (\chi_{12T})^{-1} - \chi_{13P} (\chi_{13T})^{-1}, \quad (5)$$

where χ_{12P} and χ_{13P} are the power coefficients for the ^{12}C top layer and ^{13}C bottom layer shown in Fig. 2(c), respectively, and χ_{12T} and χ_{13T} are their temperature coefficients shown in Fig. 2(b). g and κ can be solved after substituting Eq. (5) into $\Delta R_m \equiv \frac{T_{12m} - T_{13m}}{Q}$ following Eq. (4). In particular, for the three unknowns (κ_1 , κ_2 , and g), three values of ΔR_m are necessary, which can be obtained by varying the objective lenses with different r_0 .

It should be noted that the calculated g , κ_1 , and κ_2 are the overall values based on the whole temperatures measured in Fig. 2, but the value of g is considered to be the G value of the interfacial thermal conductivity between graphene layers as a constant according to the previous works [16,30]. However, the values of K_1 and K_2 are generally temperature dependent [28,31]; their values are not directly equal to κ_1 and κ_2 . Their corresponding values at different temperatures need to be obtained based on different laser powers with the assistance of obtained G .

Discussion of G and K . Substituting the data in Fig. 2(d) into the equations above, G of $105 \pm 3 \text{ MW}/(\text{m}^2 \text{ K})$ was obtained, which is in agreement with the previous simulation results [28,32–38]. Figure 3 presents the comparison of the G values of various 2D/2D interfaces. It is evident that the extracted G value of the $^{12}\text{C}/^{13}\text{C}$ BLG falls within the range of existing values, validating the constructed model above.

It is noted that the G value of the $^{12}\text{C}/^{13}\text{C}$ BLG is higher than that of other 2D heterostructures (shown in yellow) but lower than the simulated values of multilayer graphene or graphite (shown in red), which is explained as follows. The acoustic mismatch model (AMM) indicates that G is proportional to the product of phonon transmission Trans. at the interface, the overlap of the phonon density of states $\text{PDOS}_{\text{overlap}}$ between the two materials, and the derivative $\frac{df}{dT}$ of Bose-Einstein distribution function f with respect to the temperature T , near the room temperature [39].

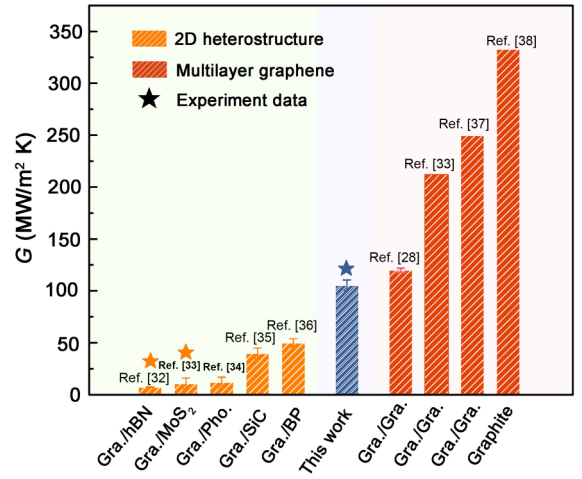


FIG. 3. Comparison of the interfacial thermal conductivity of different 2D/2D interfaces.

Therefore, G can be represented by

$$G \propto \text{Trans.} \times \text{PDOS}_{\text{overlap}} \times \frac{df}{dT}, \quad (6)$$

where Trans. is given by the density mismatch between the two materials as $\text{Trans.} \sim \min\left(\frac{\rho_1}{\rho_2}, \frac{\rho_2}{\rho_1}\right)$ in which ρ is the mass density, $\text{PDOS}_{\text{overlap}} \times \frac{df}{dT}$ can be derived from the curves of phonon density of states, and PDOS is further given by $\text{PDOS}_{\text{ZA}} = 1/[4\pi(\sigma/\rho)^{1/2}]$ in 2D materials in which σ is the flexural rigidity. As shown in Table S2 [23], the normalized G values of ^{12}C MLG and ^{13}C MLG are the highest because of their identical atomic and electronic structures [40,41]. On the other hand, it has been reported that G increases with the number of graphene layers [28,39], which agrees well with the lower G observed in $^{12}\text{C}/^{13}\text{C}$ BLG compared with the multilayer graphene or graphite. In order to express the anisotropic thermal property later, the G is artificially rewritten as k_{\perp} of $\sim 0.1 \text{ W}/(\text{m K})$ based on the relation $G = k_{\perp}/Nd$ [42], where $Nd = 0.69 \text{ nm}$ is the total thickness of BLG [43].

Furthermore, the temperature-dependent K of each layer in $^{12}\text{C}/^{13}\text{C}$ BLG were derived based on G , as shown in Fig. 4. For comparison, ^{12}C and ^{13}C MLG were also measured. It is important to clarify that the lower K of the ^{13}C layer compared to the ^{12}C layer is reasonable here, as the $^{13}\text{CH}_4$ precursor has a higher isotope doping level (as described in the Preparation details), which shortens the phonon lifetime in the resultant ^{13}C graphene [18]. As expected, all K values decrease with increasing temperature due to the enhanced umklapp scattering of phonons [30], and this is also the reason why K needs to be further derived based on the constant G mentioned above. However, the ^{12}C top layer and the ^{13}C bottom layer in $^{12}\text{C}/^{13}\text{C}$ BLG exhibit weaker temperature dependence and lower K values compared to the MLGs, probably due to a shortened phonon lifetime caused by more phonon scattering channels in BLG [44,45]. The declines in the individual layers of $^{12}\text{C}/^{13}\text{C}$ BLG show slight variations (e.g., the decrease percentages of ^{12}C and ^{13}C layers around $T \approx 350 \text{ K}$ are 20.7% and 31.1%, respectively), indicating the potential for individual control of K through the coregulation by van der Waals forces and isotopes in BLG. These findings are

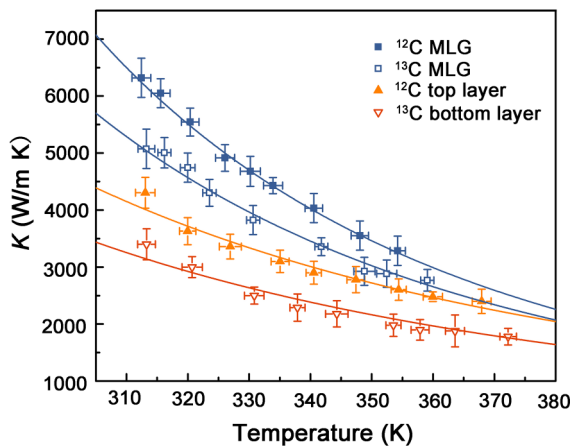


FIG. 4. The in-plane thermal conductivity of suspended CVD graphene, including ^{12}C MLG, ^{13}C MLG, and individual layers of $^{12}\text{C}/^{13}\text{C}$ BLG.

interesting and deserve further study in the future. The overall thermal conductivity anisotropy ratio $\rho = k/k_{\perp}$ between the in-plane thermal conductivity (k) and the interfacial thermal conductivity (k_{\perp}) is on the order of 10^4 , highlighting the significant potential of BLG in the field of thermal management.

Conclusion. We present a unique approach to simultaneously investigate the interfacial and in-plane thermal

conductivity of AB-stacked BLG by isotope-labeling Raman spectroscopy. The results demonstrate that isotopically labeled AB-stacked BLG has remarkably high interfacial thermal conductivity, which is attributed to the excellent crystal lattice match between the two layers. Interestingly, the in-plane thermal conductivity of each layer in isotopically labeled AB-stacked BLG is significantly reduced compared to its monolayers, and the extent of reduction varies with each layer, indicating the potential for individual control of in-plane thermal conductivity. The thermal conductivity anisotropy ratio of isotopically labeled AB-stacked BLG is found to be on the order of 10^4 , highlighting its prospect for thermal management applications. We expect this thermal measurement method as well as the corresponding heat diffusion model can be extended to more 2D systems and help in understanding the phonon mechanisms of 2D materials.

Acknowledgment. This work was financially supported by the National Science Foundation of China (Grant No. 12272336) and Zhejiang Provincial Natural Science Foundation (Grant No. LR22A0004).

Y.Z. initiated the research and conducted the experiments. Q.R. contributed to the establishment of the heat diffusion equations. J.F. assisted in conducting experiments. J.L. helped with the preparation of the samples. S.W. and J.S. provided equipment assistance and technical support in SEM characterizations. P.Z. designed, guided, and supervised the whole project. All authors commented on the Letter.

The authors declare no competing interests.

- [1] Y. Cao, V. Fatemi, S. Fang, K. Watanabe, T. Taniguchi, E. Kaxiras, and P. Jarillo-Herrero, Unconventional superconductivity in magic-angle graphene superlattices, *Nature (London)* **556**, 43 (2018).
- [2] A. A. Balandin, Thermal properties of graphene and nanostructured carbon materials, *Nat. Mater.* **10**, 569 (2011).
- [3] A. A. Balandin, Phononics of graphene and related materials, *ACS Nano* **14**, 5170 (2020).
- [4] A. Righi, S. D. Costa, H. Chacham, C. Fantini, P. Venezuela, C. Magnuson, L. Colombo, W. S. Bacsa, R. S. Ruoff, and M. A. Pimenta, Graphene moiré patterns observed by umklapp double-resonance Raman scattering, *Phys. Rev. B* **84**, 241409(R) (2011).
- [5] W. Ren, Y. Ouyang, P. Jiang, C. Yu, J. He, and J. Chen, The impact of interlayer rotation on thermal transport across graphene/hexagonal boron nitride van der Waals heterostructure, *Nano Lett.* **21**, 2634 (2021).
- [6] N. Bonini, M. Lazzeri, N. Marzari, and F. Mauri, Phonon anharmonicities in graphite and graphene, *Phys. Rev. Lett.* **99**, 176802 (2007).
- [7] E. H. Hwang and S. Das Sarma, Acoustic phonon scattering limited carrier mobility in two-dimensional extrinsic graphene, *Phys. Rev. B* **77**, 115449 (2008).
- [8] J. Ek-Weis, S. Costa, O. Frank, and M. Kalbac, Heating isotopically labeled bernal stacked graphene: A Raman spectroscopy study, *J. Phys. Chem. Lett.* **5**, 549 (2014).
- [9] M. T. Pettes, I. S. Jo, Z. Yao, and L. Shi, Influence of polymeric residue on the thermal conductivity of suspended bilayer graphene, *Nano Lett.* **11**, 1195 (2011).
- [10] P. Jiang, X. Qian, X. Gu, and R. Yang, Probing anisotropic thermal conductivity of transition metal dichalcogenides MX_2 ($M = \text{Mo}, \text{W}$ and $X = \text{S}, \text{Se}$) using time-domain thermoreflectance, *Adv. Mater.* **29**, 1701068 (2017).
- [11] H. Zhang, X. Chen, Y.-D. Jho, and A. J. Minnich, Temperature-dependent mean free path spectra of thermal phonons along the c -axis of graphite, *Nano Lett.* **16**, 1643 (2016).
- [12] G. Zhu, J. Liu, Q. Zheng, R. Zhang, D. Li, D. Banerjee, and D. G. Cahill, Tuning thermal conductivity in molybdenum disulfide by electrochemical intercalation, *Nat. Commun.* **7**, 13211 (2016).
- [13] Y. Wang, J. Y. Park, Y. K. Koh, and D. G. Cahill, Thermoreflectance of metal transducers for time-domain thermoreflectance, *J. Appl. Phys.* **108**, 043507 (2010).
- [14] D. Rodin and S. K. Yee, Simultaneous measurement of in-plane and through-plane thermal conductivity using beam-offset frequency domain thermoreflectance, *Rev. Sci. Instrum.* **88**, 014902 (2017).
- [15] A. A. Balandin, S. Ghosh, W. Z. Bao, I. Calizo, D. Teweldebrhan, F. Miao, and C. N. Lau, Superior thermal conductivity of single-layer graphene, *Nano Lett.* **8**, 902 (2008).
- [16] W. W. Cai, A. L. Moore, Y. W. Zhu, X. S. Li, S. S. Chen, L. Shi, and R. S. Ruoff, Thermal transport in suspended and supported monolayer graphene grown by chemical vapor deposition, *Nano Lett.* **10**, 1645 (2010).
- [17] S. S. Chen, A. L. Moore, W. W. Cai, J. W. Suk, J. H. An, C. Mishra, C. Amos, C. W. Magnuson, J. Y. Kang, L. Shi *et al.*, Raman measurements of thermal transport in suspended

- monolayer graphene of variable sizes in vacuum and gaseous environments, *ACS Nano* **5**, 321 (2011).
- [18] S. Chen, Q. Wu, C. Mishra, J. Kang, H. Zhang, K. Cho, W. Cai, A. A. Balandin, and R. S. Ruoff, Thermal conductivity of isotopically modified graphene, *Nat. Mater.* **11**, 203 (2012).
- [19] S. Karak, J. Bera, S. Paul, S. Sahu, and S. Saha, Low thermal conductivity and interface thermal conductance in SnS₂, *Phys. Rev. B* **104**, 195304 (2021).
- [20] J.-U. Lee, D. Yoon, H. Kim, S. W. Lee, and H. Cheong, Thermal conductivity of suspended pristine graphene measured by Raman spectroscopy, *Phys. Rev. B* **83**, 081419(R) (2011).
- [21] J. Liu, X. Zhang, S. Zhang, Z. Zou, Z. Zhang, Z. Wu, Y. Xia, Q. Li, P. Zhao, and H. Wang, Sequential growth and twisted stacking of chemical-vapor-deposited graphene, *Nanoscale Adv.* **3**, 983 (2021).
- [22] Y. Zhang, Q. Ren, X. Zhang, Z. Chen, H. Zheng, J. Liu, Y. Jin, C.-T. Lin, Y. Zhao, and P. Zhao, Facile graphene transfer using commercially available liquid bandage, *ACS Appl. Nano Mater.* **4**, 7272 (2021).
- [23] See Supplemental Material at <http://link.aps.org/supplemental/10.1103/PhysRevB.109.L041407> for the further characterization of bilayer graphene and laser diameter, the detailed equation calculation process, discussion of strain and air disturbance factors, and comparison of normalized G values of various graphene/2D interfaces. The Supplemental Material also contains Refs. [46–55].
- [24] I. Calizo, A. A. Balandin, W. Bao, F. Miao, and C. N. Lau, Temperature dependence of the Raman spectra of graphene and graphene multilayers, *Nano Lett.* **7**, 2645 (2007).
- [25] X. Li, W. Cai, L. Colombo, and R. S. Ruoff, Evolution of graphene growth on Ni and Cu by carbon isotope labeling, *Nano Lett.* **9**, 4268 (2009).
- [26] A. C. Ferrari, J. C. Meyer, V. Scardaci, C. Casiraghi, M. Lazzeri, F. Mauri, S. Piscanec, D. Jiang, K. S. Novoselov, S. Roth *et al.*, Raman spectrum of graphene and graphene layers, *Phys. Rev. Lett.* **97**, 187401 (2006).
- [27] W. Fang, A. L. Hsu, R. Caudillo, Y. Song, A. G. Birdwell, E. Zakar, M. Kalbac, M. Dubey, T. Palacios, M. S. Dresselhaus *et al.*, Rapid identification of stacking orientation in isotopically labeled chemical-vapor grown bilayer graphene by Raman spectroscopy, *Nano Lett.* **13**, 1541 (2013).
- [28] X. Nie, L. Zhao, S. Deng, Y. Zhang, and Z. Du, How interlayer twist angles affect in-plane and cross-plane thermal conduction of multilayer graphene: A non-equilibrium molecular dynamics study, *Int. J. Heat Mass Transfer* **137**, 161 (2019).
- [29] L. M. Malard, K. Fai Mak, A. H. Castro Neto, N. M. R. Peres, and T. F. Heinz, Observation of intra- and inter-band transitions in the transient optical response of graphene, *New J. Phys.* **15**, 015009 (2013).
- [30] A. Alofi and G. P. Srivastava, Thermal conductivity of graphene and graphite, *Phys. Rev. B* **87**, 115421 (2013).
- [31] A. Sood, C. Sievers, Y. C. Shin, V. Chen, S. Chen, K. K. H. Smithe, S. Chatterjee, D. Donadio, K. E. Goodson, and E. Pop, Engineering thermal transport across layered graphene-MoS₂ superlattices, *ACS Nano* **15**, 19503 (2021).
- [32] C.-C. Chen, Z. Li, L. Shi, and S. B. Cronin, Thermal interface conductance across a graphene/hexagonal boron nitride heterojunction, *Appl. Phys. Lett.* **104**, 081908 (2014).
- [33] Z. Ding, Q.-X. Pei, J.-W. Jiang, W. Huang, and Y.-W. Zhang, Interfacial thermal conductance in graphene/MoS₂ heterostructures, *Carbon* **96**, 888 (2016).
- [34] Y. Hong, J. Zhang, and X. C. Zeng, Interlayer thermal conductance within a phosphorene and graphene bilayer, *Nanoscale* **8**, 19211 (2016).
- [35] M. S. Islam, I. Mia, A. S. M. J. Islam, C. Stampfl, and J. Park, Temperature and interlayer coupling induced thermal transport across graphene/2D-SiC van der Waals heterostructure, *Sci. Rep.* **12**, 761 (2022).
- [36] Y. Chen, Y. Zhang, K. Cai, J. Jiang, J.-C. Zheng, J. Zhao, and N. Wei, Interfacial thermal conductance in graphene/black phosphorus heterogeneous structures, *Carbon* **117**, 399 (2017).
- [37] Z. Wei, Z. Ni, K. Bi, M. Chen, and Y. Chen, Interfacial thermal resistance in multilayer graphene structures, *Phys. Lett. A* **375**, 1195 (2011).
- [38] Z. Li, Y. Liu, L. Lindsay, Y. Xu, W. Duan, and E. Pop, Size dependence and ballistic limits of thermal transport in anisotropic layered two-dimensional materials, [arXiv:1711.02772](https://arxiv.org/abs/1711.02772).
- [39] S. Vaziri, E. Yalon, M. M. Rojo, S. V. Suryavanshi, H. Zhang, C. J. McClellan, C. S. Bailey, K. K. H. Smithe, A. J. Gabourie, V. Chen *et al.*, Ultrahigh thermal isolation across heterogeneously layered two-dimensional materials, *Sci. Adv.* **5**, eaax1325 (2019).
- [40] E. del Corro, M. Kalbac, C. Fantini, O. Frank, and M. A. Pimenta, Isotopic ¹³C / ¹²C effect on the resonant Raman spectrum of twisted bilayer graphene, *Phys. Rev. B* **88**, 155436 (2013).
- [41] Q.-X. Pei, Y.-W. Zhang, Z.-D. Sha, and V. B. Shenoy, Carbon isotope doping induced interfacial thermal resistance and thermal rectification in graphene, *Appl. Phys. Lett.* **100**, 101901 (2012).
- [42] S. E. Kim, F. Mujid, A. Rai, F. Eriksson, J. Suh, P. Poddar, A. Ray, C. Park, E. Fransson, Y. Zhong *et al.*, Extremely anisotropic van der Waals thermal conductors, *Nature (London)* **597**, 660 (2021).
- [43] P. Nemes-Incze, Z. Osvath, K. Kamaras, and L. P. Biro, Anomalies in thickness measurements of graphene and few layer graphite crystals by tapping mode atomic force microscopy, *Carbon* **46**, 1435 (2008).
- [44] D. Singh, J. Y. Murthy, and T. S. Fisher, Mechanism of thermal conductivity reduction in few-layer graphene, *J. Appl. Phys.* **110**, 044317 (2011).
- [45] H. Y. Li, H. Ying, X. P. Chen, D. L. Nika, A. I. Cocemasov, W. W. Cai, A. A. Balandin, and S. S. Chen, Thermal conductivity of twisted bilayer graphene, *Nanoscale* **6**, 13402 (2014).
- [46] B. N. Persson, A. I. Volokitin, and H. Ueba, Phononic heat transfer across an interface: Thermal boundary resistance, *J. Phys.: Condens. Matter* **23**, 045009 (2011).
- [47] Y. Wei, B. Wang, J. Wu, R. Yang, and M. L. Dunn, Bending rigidity and Gaussian bending stiffness of single-layered graphene, *Nano Lett.* **13**, 26 (2013).
- [48] G. Wang, Z. Dai, J. Xiao, S. Feng, C. Weng, L. Liu, Z. Xu, R. Huang, and Z. Zhang, Bending of multilayer van der Waals materials, *Phys. Rev. Lett.* **123**, 116101 (2019).
- [49] J. W. Jiang, Z. Qi, H. S. Park, and T. Rabczuk, Elastic bending modulus of single-layer molybdenum disulfide (MoS₂): Finite thickness effect, *Nanotechnology* **24**, 435705 (2013).

- [50] N. Wei, Y. Chen, Y. Zhang, C. Zhou, X. Hao, K. Xu, K. Cai, and J. Chen, Efficient selection methods for black phosphorene nanoribbons, *Nanoscale* **10**, 4385 (2018).
- [51] Q. Cai, D. Scullion, W. Gan, A. Falin, S. Zhang, K. Watanabe, T. Taniguchi, Y. Chen, E. J. G. Santos, and L. H. Li, High thermal conductivity of high-quality monolayer boron nitride and its thermal expansion, *Sci. Adv.* **5**, eaav0129 (2019).
- [52] T. M. G. Mohiuddin, A. Lombardo, R. R. Nair, A. Bonetti, G. Savini, R. Jalil, N. Bonini, D. M. Basko, C. Galotit, N. Marzari *et al.*, Uniaxial strain in graphene by Raman spectroscopy: G peak splitting, Grüneisen parameters, and sample orientation, *Phys. Rev. B* **79**, 205433 (2009).
- [53] J. Ristein, Surface transfer doping of semiconductors, *Science* **313**, 1057 (2006).
- [54] E. Kreyszig, *Advanced Engineering Mathematics*, 4th ed. (John Wiley & Sons, 1979).
- [55] Y. Wang, Y. Wang, C. Xu, X. Zhang, L. Mei, M. Wang, Y. Xia, P. Zhao, and H. Wang, Domain-boundary independency of Raman spectra for strained graphene at strong interfaces, *Carbon* **134**, 37 (2018).